Sensors & Actuators: B. Chemical 329 (2021) 129253

Contents lists available at ScienceDirect

Sensors and Actuators: B. Chemical

journal homepage: www.elsevier.com/locate/snb

Effects of donor density on power-law response in tin dioxide gas sensors

D.A. Mirabella [a], P.M. Desimone [a], M.A. Ponce [a], C.M. Aldao [a,*], L.F. da Silva [b], A.C. Catto [b], E. Longo [c]

[a] Institute of Materials Science and Technology (INTEMA), University of Mar Del Plata and National Research Council (CONICET), Juan B. Justo 4302, B7608FDQ, Mar Del Plata, Argentina
[b] Laboratory of Nanostructured Multifunctional Materials, Department of Physics, Federal University of Sao Carlos, 13565-905, São Carlos, SP, Brazil
[c] Federal University of São Carlos (UFSCar), Department of Chemistry, 13565-905, São Carlos, SP, Brazil

ARTICLE INFO

Keywords:
Semiconductor gas sensors
SnO_2
Conductivity
Chemisorption
Adsorption isotherms

ABSTRACT

We investigated the power-law responses in two types of tin dioxide (SnO_2) films: one made from nanosized grains and another from from very large grains, both under dry air. Experimental results revealed a significant dependence between the sensitivity and the SnO_2 grain size. We therefore propose, that the gas sensor sensitivity is not only determined by oxygen chemisorption, but also by changes in the density of oxygen vacancies in response to changes in the ambient gas pressure. Band bendings and adsorbate coverages for different oxygen pressures were derived resorting to the electroneutrality condition, including changes in the concentration of oxygen vacancies within the grains due to the exposure to different oxygen pressure. The consequences for the film conductivity and its power-law response were analyzed and compared with experimental results.

1. Introduction

Polycrystalline metal-oxide semiconductors (MOXs) are widely employed for gas-sensing applications, including detection of toxic gases, monitoring of emissions from vehicles, as well as in food industry to an inspection of food quality by odor [1–5]. In gas sensors based on MOX, the signal detection comes from the change of material resistivity after the interaction between the MOX surface and the target gas molecules. There is a broad consensus that the conductivity of MOX, in particular tin dioxide (SnO_2), is mainly controlled by Schottky-type intergranular barriers for grains that are large enough [6,7]. Under target gas exposure, a fraction of the adsorbed particles chemisorbs, trapping electronic carriers from the bulk, thus creating a space charge layer that changes the intergranular barrier height eV_s and consequently the electrical resistance of the sensing material. On the other hand, the bulk electrical conductivity is mainly controlled by imperfections in its crystalline structure. According to the literature, MOXs possess a high density of native point defects, oxygen vacancies, which form spontaneously and constitute the main source of doping [8–11]. For nanosized grains, depletion regions tend to overlap to the point that bands at the grain are practically flat and there is no band bending.

It has been regularly observed that the electrical resistance (R), or conductance (G), of the MOXs obeys a power-law response with gas pressure ($G \propto p^{-\gamma}$). The parameter γ determines the sensitivity of the gas sensor, defined as the slope of response against gas concentration in logarithmic scale as follows:

$$\gamma = -\frac{d\ln G}{d\ln p} \tag{1}$$

Eq. (1) is regularly expressed as:

$$\gamma = -\left(\frac{1}{G}\frac{dG}{dV_s}\right)\left(p\frac{dV_s}{dp}\right) \tag{2}$$

revealing that the sensor sensitivity has two contributions. The first term of the RHS of Eq(2), $G^{-1}dG/V_s$, is known as the *transducer function,* which relates the conductivity behavior to the barrier height transducing the chemical signal into a change of the electrical resistance. The second term, pdV_s/dp, accounts for changes in the barrier height due to the charge transfer process between the adsorbed gas molecules and the semiconductor, known as the *receptor function*.

The receptor function depends on how oxygen adsorbs at the MOX surface since it alters the intergranular barrier heights, thus modifying the film conductivity. It is generally accepted that oxygen can adsorb non-dissociatively as O_2 or O_2^- and dissociatively as O- or O^{2-} [5]. Depending on the type of oxygen chemisorption γ can be theoretically calculated giving the values 1, 1/2 and 1/4, for O_2^-, O-, and O^{2-},

* Corresponding author.
E-mail address: cmaldao@mdp.edu.ar (C.M. Aldao).

https://doi.org/10.1016/j.snb.2020.129253
Received 28 February 2020; Received in revised form 3 July 2020; Accepted 19 November 2020
Available online 27 November 2020

respectively.

Several experimental investigations reported γ values varying from 0.25 to 0.61 [12–14] for SnO_2 under air exposure. Researchers have attributed these different results to the presence of humidity in the environment responsible for spoiling the sensor. In this regard, Yamazoe and coworkers studied the sensor response under dry and humid air exposures. They used very small grains (of *ca.* 6 nm) fully depleted, and they found $\gamma = 0.25$ under dry air indicating that oxygen adsorbs exclusively as O^{2-} [15]. They also found that the value of γ increases as a function of relative humidity, tending to ½. They proposed that when humidity is present, oxygen adsorbs at the MOX surface not only as O^{2-}, but also as O-. In Refs. [15,16] and in many others, the sensor response is exclusively attributed to chemical reactions at the MOX surface. However, there is solid experimental evidence indicating that, at the usual working temperatures, the concentration of oxygen vacancies within the grains changes in response to the pressure of the target gas [17].

We investigated the power-law responses under dry air for two types of SnO_2 films: one made from nanosized grains and another from large grains (average grain size of 3 μm). We found a significant dependence between the sensitivity and the grain size. Based on these findings, we propose that the gas sensor sensitivity is not only determined by oxygen chemisorption, but also by changes in the density of oxygen vacancies in response to changes in ambient pressure, something that has not been taken into account before. To accomplish this goal, and after presenting the experimental results, in Section 3 we develop a theoretical framework in which we calculate adsorbate coverages for different oxygen pressures using the Wolkenstein theory [18]. Band bendings are determined from adsorbate coverages resorting to the electroneutrality condition assuming constant doping. Using these calculations, in Section 4 we find that the conductivity is directly proportional to $p^{-1/4}$ for small grains [15]. In Section 5, we show that the conductivity, for large grains with constant bulk doping, does not depend on gas pressure exactly as $p^{-1/4}$, but it presents a small reduction in the exponent due to changes of the depletion width. Finally, in Section 6 we extend our calculations to take into account the effects of a variable doping, *i.e.* a density of oxygen vacancies that changes as a function of ambient pressure.

2. Experimental results

A commercial high-purity SnO_2 powder (Sigma-Aldrich Company, 99.9 %, < 325 mesh) was used to prepare a sensing layer in this study. In order to increase the grain size, the as-received powder was annealed in an electric furnace under dry air atmosphere for 4 h at 1500 °C. At the end of this process, a powder with large particle size ranging from 1.25 to 5.25 μm was then obtained, as seen in Fig. 1. The FEG-SEM analyses were performed in a field emission gun scanning electron microscope (Zeiss Supra35), operated at 5 kV in different magnifications. To compare the theory with the experiments, we chose a polycrystalline film with large grains (LGF) to avoid complete depletion, so that a bulk region exists in the middle of the grains. Thus, with grain size far larger than the depletion width, the Schottky approximation is suitable.

We also made polycrystalline films from small-sized grains that achieve complete depletion (SGF), so that a bulk region does not exist in the middle of the grains. SnO_2 nanoparticles were obtained by the hydrolysis of tin chloride dehydrate. The synthesis procedure is described in Ref. [19].

For small-sized grain particles, HR-TEM analyses of the as-prepared materials were performed using a FEI microscope Tecnai G2TF20 operating at 200 kV. The HR-TEM images of these samples revealed microstructures consisting of SnO_2 nanoparticles, with an average size of 5.5 nm in diameter. The interplanar distance in the SnO_2 nanoparticles was approximately 0.33 nm, corresponding to the (110) crystallographic plane of the rutile SnO_2 phase [20].

After the thermal treatment, a slurry was prepared by mixing the SnO_2 powder with glycerol used as the organic binder. The ratio of the solid:organic binder used was 1:2, without any dopants. The thick film was prepared by the screen-printing technique onto an insulating alumina substrate (96 % dense) with electrodes consisting of an adhesion layer of titanium (25-nm thick) and a platinum film (200 nm thick). An interdigitated shape, with Pt electrodes separated by a distance of 20 μm, was delineated by using a laser micro-machine, as described elsewhere [17]. After the substrate was painted, the films were dried in a stove at 100 °C in dry air atmosphere for 24 h to evaporate the binder and to improve the adhesion of the films onto the alumina substrate. Afterwards, the films were thermally treated in an electric furnace up to 380 °C in air and maintained at this temperature for 2 h with a heating rate of 1 °C/min, to evaporate the residual binder and/or any impurity present. Raman spectrum was acquired in a Renishaw In *via* Reflex system equipped with an Argon laser line (514 nm) using a nominal power of 50 mW used as the excitation source. Fig. 2 shows the Raman bands characteristics of SnO_2. The position of the main peak at around 633 cm^{-1}, also observed by Sangeetha and co-workers [21], suggests a low concentration of defects at surface sites. The sample surface was investigated using a ScientaOmicron X-ray photoelectron spectrometer (XPS, Thermo Scientific K-Alpha spectrometer; Al-Kα radiation). The binding energies were corrected for charging effects by assigning a value of 284.8 eV to the adventitious C 1s line. In the XPS spectra, shown in Fig. 3, only Sn, C, and O were identified at the surface of both samples (large and small grains). Thus, the presence of any impurities was below the detection capability of these techniques.

Oxygen-sensing electrical measurements were performed using synthetic dry air (Air Products Brazil Cod 196514, 21 % O_2, 79 % N_2, 3

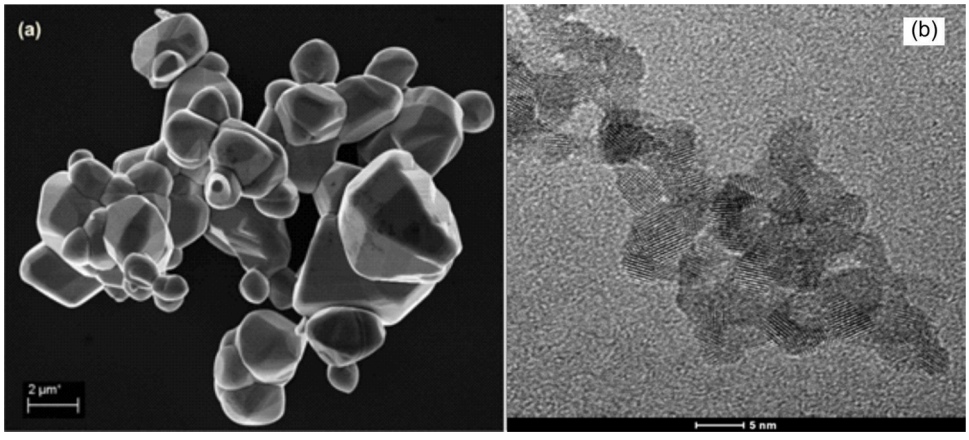

Fig. 1. a) FEG-SE micrography of the SnO_2 powder after annealing treatment at 1500 °C, large grains. (b) HR-TEM micrography of the SnO_2 powder before the annealing treatment, small grains.

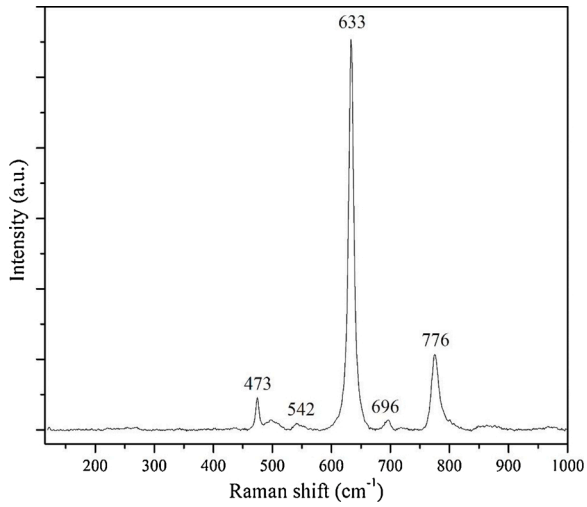

Fig. 2. Raman spectrum of the SnO_2 sample exhibiting large grains films after thermal treatment up to 380 °C in dry air atmosphere.

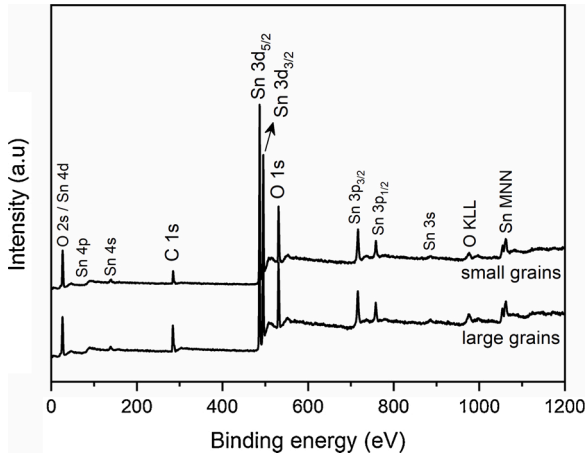

Fig. 3. XPS spectra of the SnO_2 samples (exhibiting large and, small grains) revealing the presence of only Sn, C, and O atoms at the surface of the samples.

ppm H_2O, purity of 99.99 %) maintaining a constant total flow of 300 SCCM *via* mass flow controllers (Cole-Parmer). Measurements were carried out under different dry air concentrations varying from 0.007 to 1 atm. The samples were tested in a dynamic chamber with controlled temperature and gas composition, as shown in Fig. 4. The electrical characterization was performed using a Keithley 2400 source/measure unit. The temperature was set to 300 °C, an usual temperature used in gas sensing, and the electrical resistance of the film was measured after successive increments of air partial pressure. DC electrical measurements were collected in an electrometer (Keithley, model 6514). These measurements were started after the samples reached steady-state at each air partial pressure, when no changes in resistance over time were observed.

In Fig. 5, the conductance *vs.* air pressure at 300 °C is presented. Straight lines correspond to a linear fitting of the log-log experimental results. We found that $\gamma = 0.39$ for large grains, a value larger than the value found for fully depleted grains and the theoretically predicted value for doubly charged oxygen after dissociative chemisorption [15].

3. Oxygen chemisorption

Several MOXs, such as SnO_2, are naturally n-type semiconductors since oxygen vacancies are the dominant defects and they behave as

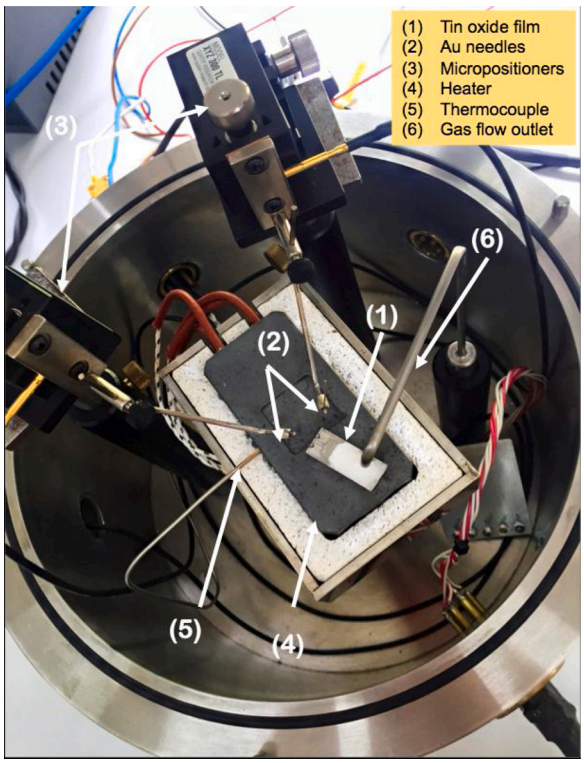

Fig. 4. Photography of the interior of the gas-sensing chamber with controlled temperature and gas level.

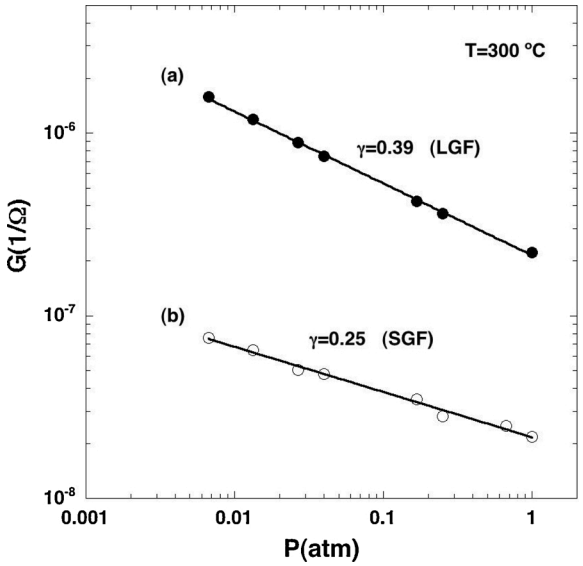

Fig. 5. Experimental SnO_2 thick film conductance as a function of air partial pressure. (a) The power-law response has exponent $\gamma = 0.39$ for large grains (LGF, average grain size of 3 μm). (b) The power-law response has exponent $\gamma = 0.25$, for fully depleted grains (SGF, average grain size of 5 nm), as predicted for doubly charged oxygen dissociative chemisorption.

donors. Sensing characteristics are believed to be due to changes in the intergranular charge after adsorption processes that directly affect its electrical conduction [11].

Depending on the relative energy position of its LUMO, lowest unoccupied molecular orbital (E_A in Fig. 6) with respect to the Fermi level E_F, adsorbed oxygen can act as an electron acceptor [18,22]. For large grains, electrons that ionize adsorbed oxygen come from the

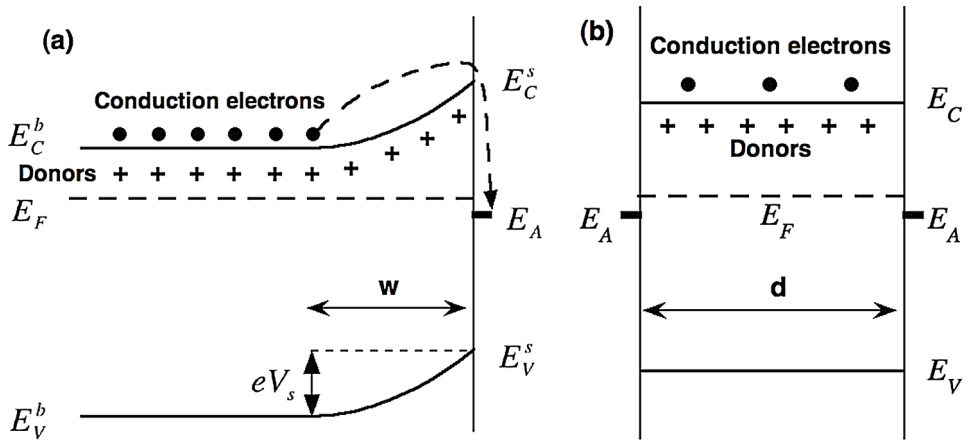

Fig. 6. 1D band scheme at an n-type semiconductor surface due to surface sites. E_C, E_V, E_F, and E_A denote the energy of the conduction band minimum, the valence band maximum, the Fermi level, and the surface site energy, respectively. (a) Large grain, where eV_s is the potential barrier or band bending, which is taken with a positive value and w is the width of the depletion region. (b) Fully depleted grain of width d.

semiconductor bulk, producing an electron-depleted surface region, known as the space-charge layer. The positively charged depleted region and the negatively charged surface are responsible for the band bending illustrated in Fig. 6(a). This represents a potential barrier of height eV_s that electrons have to overcome to establish an electrical current. In the case of very small grains, the depletion regions are overlapped and the bands are practically flat, as seen in Fig. 6(b).

In general, the amount of adsorbed particles in equilibrium is established when the rate of adsorption is equal to the rate of desorption. Thus, we adopted the Langmuir adsorption theory, in which independent adsorption centers with the same adsorption characteristics are assumed. Also, each center can hold one gas atom or molecule, adsorbed particles do not interact among themselves, and the density of adsorption sites is independent of their occupancy with no activation energy for adsorption required [18,22,23].

The possible active oxygen species at SnO_2 surface have been a long-lasting discussion. Despite controversies, it is generally accepted that oxygen can adsorb at the surface as O_2, O_2^-, O^-, or O^{2-} [5,24–29]. Yamazoe and co-workers proposed that the oxygen can adsorb dissociatively as O^{2-} in dry air, and as O^- or O^{2-} in the presence of humidity [15]. Despite the fact that oxygen incorporation into the surface can be more complicated than it is regularly assumed in phenomenological models [30,31], oxygen at the surface is responsible for the creation of electron acceptor sites needed to account for band bending.

When analyzing dissociative chemisorption and desorption, we must take into account that the gas phase particles are dioxygen molecules, while the surface adsorbates consist of single oxygen atoms, which can be neutral or charged. If only neutral adsorbed species can desorb [23], the surface coverage Θ for dissociative chemisorption adopts the form

$$\Theta = \frac{\sqrt{\beta p}}{1+\sqrt{\beta p}}, \tag{3}$$

with

$$\beta = \beta_0 \left[1 + \exp\left(2\frac{E_F - E_A}{kT}\right)\right]^2$$

for double acceptor levels, and

$$\beta_0 = \frac{s}{N^* \nu^0 (2\pi m k T)^{1/2}} \exp\left(\frac{q^0}{kT}\right) \tag{4}$$

where p is the oxygen phase pressure, k is the Boltzmann constant, T is the temperature, q^0 is the neutral binding energy, ν^0 is the oscillation frequency of the neutral adsorbates, s is the sticking coefficient, m is the mass of the gas molecule, and N^* is the number of adsorption sites per unit surface area.

4. Power-law response for small grains

In a small grain, bands are practically flat and there is not a quasi-neutral region at the center of the grain, as shown in Fig. 6(b). The Fermi level position and the oxygen coverage as a function of temperature and pressure can be determined by resorting to the electroneutrality condition: the positive charge at the depletion region, due to oxygen vacancies, must be practically the same as the negative charge at the surface, due to chemisorbed oxygen, assuming a much smaller density of electrons within the grain. For a 1D homogeneous semiconductor, with a uniform doping concentration, the charge density due to the uncompensated doubly ionized donors is given by

$$\sigma_b = 2edN_d, \tag{5}$$

where N_d is the dopant concentration and d is the width, as shown in Fig. 6(b). On the other hand, the negative charge at the surface for doubly charged acceptors due to oxygen adsorption is given by:

$$\sigma_s = 2eN^* \Theta^{2-}, \tag{6}$$

where Θ^{2-} is the coverage of doubly charged adsorbates, which is obtained as $f\Theta$ (where f is the Fermi-Dirac function). Then:

$$\sigma_s = 2eN^* \beta_0^{1/2} p^{1/2} \exp[2(E_F - E_A)/kT] \tag{7}$$

Finally, the Fermi level position can be determined resorting to the electroneutrality condition $\sigma_s = \sigma_b$:

$$\exp[(E_F - E_A)/kT] = \left(\frac{dN_d}{N^* \beta_0^{1/2}}\right)^{1/2} p^{-1/4} \tag{8}$$

With Fig. 6(b) in mind, we can write

$$\exp[-(E_C - E_F)/kT] = \left(\frac{dN_d}{N^* \beta_0^{1/2}}\right)^{1/2} \exp[-(E_C - E_A)/kT] p^{-1/4}. \tag{9}$$

The electron density n at the conduction band is then:

$$n = N_C \left(\frac{dN_d}{N^* \beta_0^{1/2}}\right)^{1/2} \exp[-(E_C - E_A)/kT] p^{-1/4}, \tag{10}$$

where N_C is the effective density of states at the bottom of the conduction band. Assuming that the conductivity G is directly proportional to the density of carriers, we can conclude from Eq.(10) that G is proportional to $p^{-1/4}$.

5. Power-law response for large grains

In a large grain, depletion regions are not overlapped, enabling the presence of a quasi-neutral region at the center of the grain. The band bending, oxygen coverage as a function of temperature, and pressure can be determined by resorting to the electroneutrality condition: the positive charge at the depletion region, due to oxygen vacancies, must be the same as the negative charge at the surface, due to chemisorbed oxygen. For a homogeneous semiconductor, with a uniform doping concentration, the charge due to the uncompensated doubly ionized donors is given by [32–34]

$$\sigma_b = (2e\varepsilon N_d)^{1/2}\left[2V_s - \frac{kT}{e}(1-\exp(-eV_s/kT)\right]^{1/2}, \quad (11)$$

where ε is the semiconductor permittivity and N_d is the dopant concentration. On other hand, the negative charge at the surface for doubly charged acceptors due to oxygen adsorption is given by Eq.(7).

Based on Fig. 6(a), we can write:

$$E_F - E_A = (E_C^s - E_A) - eV_S - (E_C^b - E_F), \quad (12)$$

and by substituting in Eq.(7), the surface charge for a large grain can be written as:

$$\sigma_s = 2eN^*\beta_0^{1/2}p^{1/2}\exp\left[2(E_C^s - E_A)/kT\right]\exp\left[-2(E_C^b - E_F)/kT\right]\exp[-2eV_S/kT], \quad (13)$$

which explicitly shows the dependence of σ_s on band bending.

With Eqs. (11) and (13) (σ_b=σ_s), we can then obtain

$$\exp(-\Phi/kT)\propto N_d^{1/4}V_s^{1/4}p^{-1/4} \quad (14)$$

where Φ=eV_S+(E^b_C-E_F) is the barrier height. We have considered that V_s is larger than kT/e, so corrections in the right hand side of Eq.(11) are small, applying the so-called depletion approximation. If the only mechanism present for conduction is thermionic emission, (*i.e.*, the conductance is proportional to *exp(-Φ/kT))*, then from Eq.(14), for a given doping, we can write:

$$G\propto V_s^{1/4}p^{-1/4} \quad (15)$$

In Fig. 7 we present the resulting band bending for dissociative chemisorption of oxygen double acceptors. To make the calculations, we adopted typical values of the relevant parameters for SnO_2: m=0.3m_0 for the electron effective mass, $\varepsilon = 12.3\varepsilon_0$ for the electric permittivity, $N^* = 10^{19}$ m^{-2} for the adsorption sites per unit surface, and $\nu^\circ = 10^{13}$ s^{-1} for the oscillation frequencies of the adsorbates [35,36]. We fixed the energy level of chemisorption-induced states at E^s_C-E_A=1 eV [37], and the adsorption energy for a neutral particle as $q^\circ = 0.1$ eV [38–40].

In the range where thermionic emission is the dominant conduction mechanism, the parameter γ is slightly smaller than ¼ due to band bending dependence, Eq.(15). The electrical resistance of polycrystalline semiconductors such as SnO_2 has been considered to be determined by Schottky barriers at grain surfaces since years ago [41]. Thus, conduction mechanisms have been interpreted in analogy to those in metal-semiconductor contact diodes. There are two mechanisms that contribute to sample conductivity. The first mechanism is provided by electrons with energies above the top of the barrier, the *thermionic current* which is the only contribution almost exclusively reported in the literature. The second mechanism is provided by electrons with energies below the top of the barrier that can penetrate the barrier and reach the other grain by quantum-mechanical tunneling, phenomenon known as *thermionic-field emission* [42]. Interestingly, in many cases, calculations have demonstrated that most electrons cross the barrier at energies between the bulk conduction band level and the top of the barrier [43]. When the conductivity is calculated including the tunneling contribution to the electrical conduction, deviations from ideal results appear, thus reducing the γ value, as shown in Fig. 8 of the Ref. 34. Fig. 7 shows that the band bending increases linearly with the logarithm of the pressure, which can be seen for all dopings. However, from Fig. 8 we can observe that the slope of the conductivity for $N_d = 10^{24}$ m^{-3} is smaller than that for the other doping levels. This is a consequence of the tunneling contribution.

As shown in Section 2, we obtained the value γ=0.25 for small grains, as reported in Ref. [15] and consistent with the theoretically obtained results for a uniform doping concentration and doubly ionized acceptors induced by dissociative oxygen chemisorption (Section 4). In this Section, we theoretically derived γ=0.25 for large grains and a constant density of donors. Note that we used the same experimental conditions for both types of samples. However, as it can be seen in Fig. 5, we obtained a value of γ=0.39 for SnO_2 at 300 °C for LGF averaging 3 μm. Hua and co-workers reported a value of γ=0.33 and γ=0.36 for intermediate size grains, *i.e.*, 25 nm and 70 nm, respectively [46].

Evidence for oxygen in-out diffusion was reported long ago [45]. Kamp and co-workers also observed oxygen diffusion in SnO_2 monocrystals at temperatures as low as 200 °C [46]. By using impedance spectroscopy, we showed that oxygen can be incorporated into the grains of SnO_2 at relatively low temperatures [18,47]. This finding indicates that the first factor in the RHS (Eq. 14) depends on p affecting the

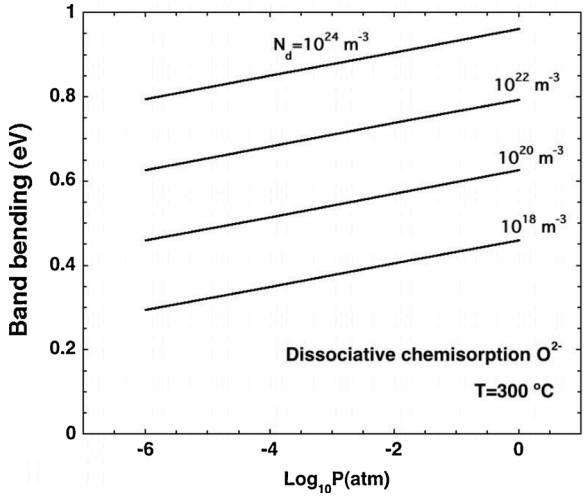

Fig. 7. Band bending due to double acceptors induced by dissociative oxygen chemisorption as a function of N_d and oxygen pressure assuming that only neutral adsorbates can desorb at T = 300 °C.

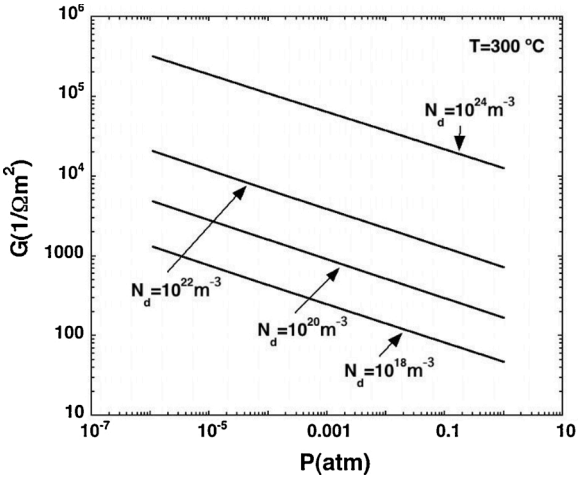

Fig. 8. Conductance as a function of oxygen pressure for different doping levels for double acceptors induced by dissociative oxygen chemisorption.

exponent γ. Therefore, we propose that the values of γ can be explained including oxygen in-out diffusion and tunneling contribution to the electrical conduction.

6. Power-law response with oxygen vacancies density depending on pressure

Native point defects due to oxygen vacancies are the main donor contribution in many oxides, particularly SnO_2. At high enough temperatures, it is expected that oxygen diffuses in and out of the grains, causing the resulting donor density distribution to have a dependence on oxygen pressure at the gas phase. Indeed, the equilibrium donor density can be directly deduced resorting to the mass action law. The oxygen exchange equilibrium between SnO_2 and the gas phase is regularly written as [8]:

$$O_0 \Leftrightarrow V^{++} + 2e^- + \frac{1}{2}O_2, \tag{16}$$

where O_0 is a neutral oxygen at the crystal, V^{++} is a doubly ionized oxygen vacancy, e^- is an electron, and O_2 is an oxygen molecule at the gas phase. Regardless of the mechanisms involved in Eq. (16), under thermodynamic equilibrium, the corresponding mass action law can be expressed as:

$$[V^{++}]n^2 p^{1/2} = const., \tag{17}$$

where square brackets denote concentration, n is the electron density, and p is the oxygen partial pressure. Assuming that all vacancies are doubly ionized, *i.e.*, $N_d \approx [V^{++}]$, Eq. (17) implies:

$$N_d = Kp^{-1/2}\exp\left[2(E_C^s - E_F)/kT\right], \tag{18}$$

where K is a constant. For small grains, using the electroneutrality condition ($\sigma_b = \sigma_s$) and introducing Eq. (18) into Eq. (5), the sensitivity on pressure does not change.

For large grains, by assuming an intrinsic behavior and doubly ionized vacancies, the charge neutrality implies $n = 2[V^{++}]$ at the quasi-neutral region at the center of the grains. Then, N_d can be expressed as:

$$N_d = Cp^{-1/6}, \tag{19}$$

where C is a constant. The value of the constant C can be calculated from oxygen vacancy densities that were determined to be around 5×10^{24} m^{-3} at relatively low pressures [8]. Maier and Gopel found that the effective donor density depends on the pressure as $p^{-1/4}$ when acceptor impurities are present (extrinsic behavior). In the absence of acceptor impurities (intrinsic behavior), N_d is directly proportional to $p^{-1/6}$ [8]. As a result, the conductivity for the first case would be slightly more sensitive to oxygen pressure. However, the main conclusions of this paper would be still the same.

Eq.(14) can be rewritten using Eq.(19) given a new value for the sensitivity γ.

$$\exp(-\Phi/kT) \propto V_s^{1/4} p^{-7/24}. \tag{20}$$

Note that when changes in the vacancy concentration are taken into account in the calculations, and assuming that the only mechanism present for conduction is thermionic emission, the resulting power-law exponent γ is 7/24 = 0.292. Values for γ even larger than this result were presented in this work, and also reported in the literature [12,13]. Motivated by these findings, we explored the consequences of including the tunneling contribution to the electrical conduction and found that the power-law exponent can be significantly altered.

In Fig. 9a we plot the conductance *vs.* pressure at 300 °C, when only the thermionic contribution (G_{th}) is taken into account and the total conductance including both thermionic and tunneling contributions (G_{tot}) for $C = 4.64 \times 10^{21}$ m^3 $atm^{1/6}$ which corresponds to a value $N_d = 10^{23}$ m^{-3} for $P = 10^{-8}$ atm. This low value of C was chosen to show the dependence of sensitivity on doping. Note that the sensitivity slightly changes (~6%) when the tunneling contribution is included since N_d is not large enough; as a result the thermionic contribution is dominant (ranging from 52 % to 79 % of the total conductance). We performed the same calculations for $C = 2.32 \times 10^{23}$ m^3 $atm^{1/6}$ corresponding to a value $N_d = 5 \times 10^{24}$ m^{-3} for $P = 10^{-8}$ atm, as shown in Fig. 9b. Note that the sensitivity does not change when only the thermionic contribution to the electrical conduction is considered, but its absolute value increases compared to the corresponding to $N_d = 10^{23}$ m^{-3} as it is expected [8,44]. However, the inclusion of the tunneling contribution has a strong effect on the sensitivity since the dominant contribution to the conductance now derives from tunneling (ranging from 65 % to 98 % of the total conductance).

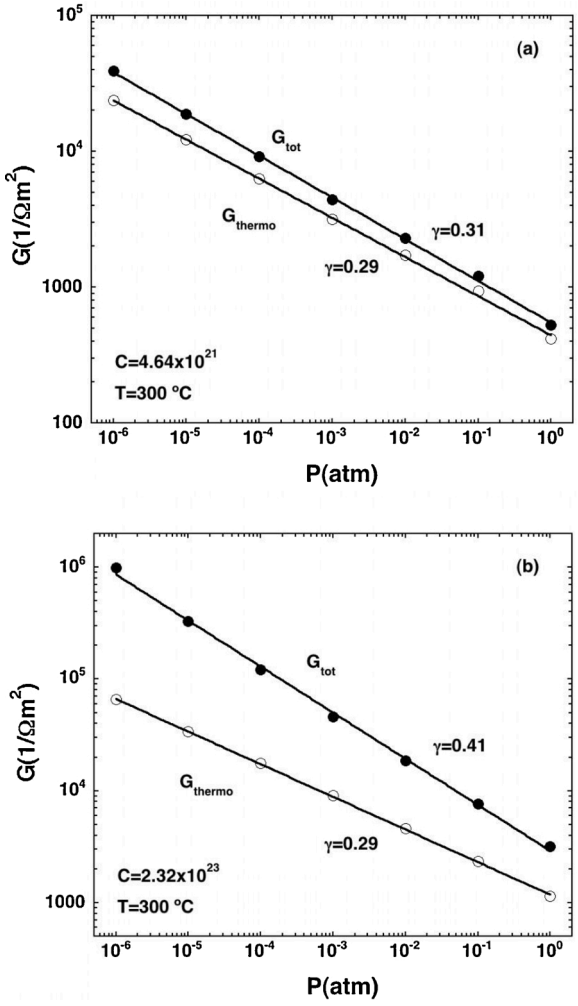

Fig. 9. (a) Conductance per square meter for $C = 4.64 \times 10^{21}$ m^3 $atm^{1/6}$ corresponding to a value $N_d = 10^{23}$ m^{-3} for $P = 10^{-8}$ atm and $T = 300$ °C, when only the thermionic contribution is taken into account ($G_{th} \sim P^{-0.29}$) and the total conductance including both thermionic and tunneling contributions ($G_{tot} \sim P^{-0.31}$). (b) Conductance per square meter for $C = 2.32 \times 10^{23}$ m^3 $atm^{1/6}$ corresponding to a value $N_d = 5 \times 10^{24}$ m^{-3} for $P = 10^{-8}$atm and $T = 300$ °C, when only the thermionic contribution is taken into account ($G_{th} \sim P^{-0.29}$) and the total conductance including both thermionic and tunnel contributions ($G_{tot} \sim P^{-0.41}$).

7. Conclusions

The power-law response of a gas sensor, based on polycrystalline SnO_2, was experimentally investigated for films presenting nanosized and large grains under the same experimental conditions. Experimental

results validated the well-known power-law, but showed different exponents, $\gamma = 0.25$ and 0.39, for films made from small and large grains, respectively. In the second case, γ was larger than the theoretically predicted value for double-charged oxygen after dissociative chemisorption ($\gamma = 0.25$). These results are very difficult to explain resorting to surface phenomena. In this work, we proposed an alternative explanation that includes the effects of donor density on the power-law response. For simplicity we performed our calculations assuming a constant density of positive charge in the depletion region, due to uniformly distributed oxygen vacancies, that can change in response to ambient oxygen partial pressure [17,47], while the negative charge at the surface was determined by deriving the adsorption isotherms for oxygen dissociative chemisorption using the Wolkenstein theory [18,32,34]. We found that the sensitivity γ is not affected in SGF. Conversely, we theoretically predict a power-law exponent $\gamma = 7/24 > 1/4$ for LGF, when the effects of donor density are taken into account in the thermionic current calculations. We also extended our calculations by including the tunneling contribution to electrical conduction and we found that the resulting power-law exponent can be even larger.

CRediT authorship contribution statement

D.A. Mirabella: Conceptualization, Methodology, Software, Formal analysis, Writing - original draft, Writing - review & editing, Visualization. **P.M. Desimone:** Investigation, Writing - review & editing, Visualization. **M.A. Ponce:** Investigation, Writing - review & editing, Funding acquisition. **C.M. Aldao:** Conceptualization, Validation, Resources, Writing - original draft, Visualization, Supervision, Project administration, Funding acquisition. **L.F. da Silva:** Conceptualization, Investigation, Resources, Writing - review & editing. **A.C. Catto:** Investigation. **E. Longo:** Conceptualization, Resources, Funding acquisition.

Declaration of Competing Interest

The authors report no declarations of interest.

Acknowledgements

This work was partially supported by the National Council for Scientific and Technical Research (CONICET) of Argentina and the National University of Mar del Plata (Argentina). The authors thank Prof. Valmor R. Mastelaro (IFSC-USP) for the XPS measurements. L. F da Silva, A. C. Catto, and E. Longo thank the financial support to FAPESP (under grants 2017/12437-5, 2018/18208-0, and 2013/07296-2), CNPq (405140/2018-5 and 426511/2018-2) and CAPES. The research was partially performed at the Brazilian Nanotechnology National Laboratory (LNNano) (Project LMF-18580) in Campinas, SP, Brazil.

References

[1] M.J. Madou, R. Morrison, Chemical Sensing With Solid State Devices, John Wiley & Sons, Inc., New York, 1989.
[2] J.W. Gardner, P.N. Bartlett, A brief history of electronic noses, Sens. Actuators B Chem. 18 (1994) 211–220.
[3] D.E. Williams, Semiconducting oxides as gas-sensitive resistors, Sens. Actuators B Chem. 57 (1999) 1–16.
[4] Il-Doo Kim, A. Rothschild, H.L. Tuller, Advances and new directions in gas-sensing devices, Acta Mater. 61 (2013) 974–1000.
[5] N. Barsan, U. Weimar, Conduction model of metal oxide gas sensors, J. Electroceram. 7 (2001) 143–167.
[6] N. Yamazoe, K. Shimanoe, Theory of power laws for semiconductor gas sensors, Sens. Actuators B Chem. 128 (2008) 566–573.
[7] N. Barsan, U. Weimar, Metal oxide-based gas sensor research: how to? Sens. Actuators B Chem. 121 (2007) 18–35.
[8] J. Maier, W. Gopel, Investigations of the bulk defect chemistry of polycrystalline tin (IV) oxide, J. Solid State Chem. 72 (1988) 293–302.
[9] S. Lany, A. Zunger, Dopability, intrinsic conductivity, and nonstoichiometry of transparent conducting oxides, Phys. Rev. Lett. 98 (2007), 045501.
[10] H.L. Tuller, S.R. Bishop, Point defects in oxides: tailoring materials through defect engineering, Annu. Rev. Mater. Res. 41 (2011) 369–398.
[11] S.R. Morrison, Mechanisms of semiconductor gas sensor operation, Sens. Actuators 11 (1987) 283–287.
[12] P.K. Clifford, D.T. Tuma, Characteristics of semiconductors gas sensors I. Steady state gas response, Sens. Actuators 3 (1982/1983) 233-254.
[13] Z. Hua, Yan Li, Yan Zeng, Yi Wu, A theoretical investigation of the power-law response of metal oxide semiconductor gas sensors I: Schottky barrier control, Sens. Actuators B Chem. 255 (2018) 1911–1919.
[14] Z. Hua, Z. Qiu, Yan Li, Yan Zeng, Yi Wu, X. Tian, M. Wang, E. Li, A theoretical investigation of the power-law response of metal oxide semiconductor gas sensors II: Size and shape effects, Sens. Actuators B Chem. 255 (2018) 3541–3549.
[15] N. Yamazoe, K. Suematsu, K. Shimanoe, Extension of receptor function theory to include two types of adsorbed oxygen for oxide semiconductor gas sensors, Sens. Actuators B Chem. 163 (2012) 128–135.
[16] S. Wicker, M. Guiltat, U. Weimar, A. Hémeryck, N. Barsan, Ambient humidity influence on CO detection with SnO_2 gas sensing materials. A combined DRIFTS/DFT investigation, J Phys Chem C 121 (2017) 25064–25073.
[17] C.M. Aldao, F. Schipani, M.A. Ponce, E. Joanni, F.J. Williams, Conductivity in SnO_2 polycrystalline thick film gas sensors: tunneling electron transport and oxygen diffusion, Sens. Actuators B Chem. 193 (2014) 428–433.
[18] T. Wolkenstein, Electronic Processes on Semiconductor Surfaces during Chemisorption, Consultants Bureau, New York, 1991.
[19] L.F. da Silva, J.-C. M'Peko, A.C. Catto, S. Bernardini, V.R. Mastelaro, K. Aguir, C. Ribeiro, E. Longo, UV-enhanced ozone gas sensing response of ZnO- SnO_2 heterojunctions at room temperature, Sens. Actuators B Chem. 240 (2017) 573–579.
[20] V. Bonu, A. Das, S. Amirthapandian, S. Dhara, A.K. Tyagi, Photoluminescence of oxygen vacancies and hydroxyl group surface functionalized SnO_2, Phys. Chem. Chem. Phys. 17 (2015) 9794–9801.
[21] P. Sangeetha, V. Sasirekha, V. Ramakrishnan, Micro-Raman investigation of tin dioxide nanostructured material based on annealing effect, J. Raman Spectrosc. 42 (2011) 1634–1639.
[22] M.E. Franke, T.J. Koplin, U. Simon, Metal and metal oxide nanoparticles in chemiresistors: does the nanoscale matter? Small 2 (2006) 36–50.
[23] H.J. Krusemeyer, D.G. Thomas, Adsorption and charge transfer on semiconductor surfaces, J. Phys. Chem. Solids 4 (1958) 78–90.
[24] T. Sahm, A. Gurlo, N. Barsan, U. Weimar, Basics of oxygen and SnO2 interaction; work function change and conductivity measurements, Sens. Actuators B Chem. 118 (2006) 78–83.
[25] N. Barsan, M. Hubner, U. Weimar, Conduction mechanisms in SnO_2 based polycrystalline thick film gas sensors exposed to CO and H_2 in different oxygen backgrounds, Sens. Actuators B Chem. 157 (2011) 510–517.
[26] M. Batzill, U. Diebold, The surface and materials science of tin oxide, Prog. Surf. Sci. 79 (2005) 47–154.
[27] U. Pulkkinen, T.T. Rantala, T.S. Rantala, V. Lantto, Kinetic Monte Carlo simulation of oxygen exchange of SnO_2 surface, J. Mol. Catal. A Chem. 166 (2001) 15–21.
[28] W. Izydorczyk, B. Adamowicz, Computer analysis of oxygen adsorption at SnO_2 thin films, Optica Applicata 37 (2007) 377–385.
[29] A. Gurlo, Interplay between O2 and SnO2: oxygen ionosorption and spectroscopic evidence for adsorbed oxygen, Chem. Phys. Chem. 7 (2006) 2041–2052.
[30] S.-C. Chang, Oxygen chemisorption on tin oxide: correlation between electrical conductivity and EPR measurements, J. Vac. Sci. Technol. 17 (1980) 366–369.
[31] J.-M. Ducéré, A. Hemeryck, A. Estève, M.D. Rouhani, G. Landa, P. Ménini, C. Tropis, A. Maisonnat, P. Fau, B. Chaudret, A computational chemist approach to gas sensors: modeling the response of SnO2 to CO, O2, and H2O gases, J. Comput. Chem. 33 (2012) 247–258.
[32] A. Rothschild, Y. Komem, Numerical computation of chemisorption isotherms for device modeling of semiconductor gas sensors, Sens. Actuators B Chem. 93 (2003) 362–369.
[33] E.H. Rhoderick, R.H. Williams, Metal-Semiconductor Contacts, Clarendon Press, Oxford, 1988. Chap. 4.
[34] D.A. Mirabella, C. Buono, C.M. Aldao, D.E. Resasco, Chemisorption and sensitivity at semiconductor sensors revisited, Sens. Actuators B Chem. 285 (2019) 232–239.
[35] S. Gomri, J.L. Seguin, J. Guerin, K. Aguir, Adsorption–desorption noise in gas sensors: modelling using Langmuir and Wolkenstein models for adsorption, Sens. Actuators B Chem. 114 (2006) 451–459.
[36] S. Gomri, J.L. Seguin, J. Guerin, K. Aguir, A mobility and free carriers density fluctuations based model of adsorption–desorption noise in gas sensor, J. Phys. D Appl. Phys. 41 (2008), 065501.
[37] S. Gomri, T. Contaret, J. Seguin, K. Aguir, M. Masmoudi, Noise modeling in MOX gas sensors, Fluctuations Noise Lett. 16 (2017), 1750013.
[38] F. Ciucci, C. de Falco, M.I. Guzman, S. Lee, T. Honda, Chemisorption on semiconductors: the role of quantum corrections on the space charge regions in multiple dimensions, Appl. Phys. Lett. 100 (2012), 183106.
[39] A. Rothschild, Y. Komem, N. Ashkenasy, Quantitative evaluation of chemisorption processes on semiconductors, J. Appl. Phys. 92 (2002) 7090–7097.
[40] A. Bejaoui, J. Guerin, J.A. Zapien, K. Aguir, Theoretical and experimental study of the response of CuO gas sensor under ozone, Sens. Actuators B Chem. 190 (2014) 8–15.
[41] W. Gopel, K. Schierbaum, SnO_2 sensors: currents status and future prospect, Sensor. Actuator. B: Chem. 26 (1995) 1–12.
[42] E.H. Rhoderick, R.H. Williams, Metal-Semiconductor Contacts, Clarendon Press, Oxford, 1988. Chap. 3.
[43] C.R. Crowell, V.L. Rideout, Normalized thermionic-field (T-F) emission in metal-semiconductor (Schottky) barriers, Solid-State Electron. 12 (1969) 89–105.

[44] Z. Hua, C. Tian, D. Huang, W. Yuan, C. Zhang, X. Tian, M. Wang, E. Li, Power-law response of metal oxide semiconductor gas sensors to oxygen in presence of reducing gases, Sens. Actuators B Chem. 267 (2018) 510–518.
[45] G. Blaustein, M.S. Castro, C.M. Aldao, Influence of frozen distributions of oxygen vacancies on tin oxide conductance, Sens. Actuator. B: Chem. 55 (1999) 33–37.
[46] B. Kamp, R. Merkle, J. Maier, Chemical diffusion of oxygen in tin dioxide, Sens. Actuators B Chem. 77 (2001) 534–542.
[47] F. Schipani, M.A. Ponce, E. Joanni, F.J. Williams, C.M. Aldao, Study of the oxygen vacancies changes in SnO_2 polycrystalline thick films using impedance and photoemission spectroscopies, J. App. Phys. 116 (2014), 194502.

Daniel A. Mirabella received his B.Sc. in Computer Science in 1998 from CAECE University of Mar del Plata. He is nowadays Assistant Professor at the University of Mar del Plata. His research activities focus on surface growth and physic-chemistry of semiconductor surfaces and interfaces.

Mariela Desimone received her B.Sc. in 2007 and her Ph.D. in Materials Science in 2013 at the University of Mar del Plata, Argentina. Since 2011 she is a member of the staff of the National Research Council (CONICET). She currently holds a researcher position at the Institute of Materials Science and Technology (INTEMA). Her research interests are focused to the electronic properties and conduction mechanisms of metal oxide semiconductors based gas sensors.

Miguel A. Ponce obtained his B.Sc. in Chemistry in 1999 and his PhD in Material Science in 2005 from Mar del Plata National University, Argentina. Since April 2007 he is a member of the research staff of the National Research Council (CONICET). His current research interests include the development of electronic conduction mechanism of functional inorganic materials, the conduction mechanisms and electrical properties of thick films based on semiconductor oxides.

Celso M. Aldao completed his Ph.D. at the Department of Chemical Engineering and Materials Science of the University of Minnesota in 1989. He was appointed as Professor in 1990 at the University of Mar del Plata. Since 1992 he is a member of the research staff of the National Research Council (CONICET). He specializes in the physics and chemistry of surfaces and interfaces, with special emphasis on semiconductors.

Luís Fernando da Silva is currently professor at Department of Physics, Federal University of São Carlos, Brazil. He received his PhD in Materials and Engineering from São Carlos School of Engineering, University of São Paulo (Brazil) with a Post-doctoral fellowship in the Laboratory for Multifunctional Materials, Department of Materials, at ETH Zürich, Switzerland. His research interests mostly deal with synthesis of oxide compounds *via* chemical methods and the characterization of these compounds by X-ray absorption spectroscopy (XAS), photoluminescence, transmission and scanning electron microscopy, and the electrical gas sensing properties of these oxide compounds.

Ariadne Cristina Catto is currently post-doctor at Federal University of São Carlos (UFSCar), Brazil with a fellowship from São Paulo Research Foundation (FAPESP). She received her PhD in Materials and Engineering from São Carlos School of Engineering, University of São Paulo (Brazil). Her research interests mostly deal with synthesis of oxide compounds and the characterization of these compounds with X-ray photoelectron spectroscopy (XPS) and their gas sensing performance.

Elson Longo is Emeritus Professor at the Department of Chemistry of the Federal University of São Carlos, Brazil (UFSCar). He is also Professor HONORIS CAUSA at the Federal University of Paraiba. He received his PhD in Physical Chemistry from the USP-São Carlos Institute of Physics. He has published over 1200 articles in international journals, with an h-index of 72, and 26,545 citations. He has 32 privilege requests and has generated over 980 congress papers in the last 13 years. He developed more than 42 projects and agreements with the Federal and State governments.